Planning and Control of a Nonholonomic Unicycle using Ring Shaped Local Potential Fields

Kaustubh Pathak, Graduate Student
Mechanical Systems Lab
Department of Mechanical Engineering
University of Delaware, Newark DE 19716.
Email: pathak@me.udel.edu

Sunil K. Agrawal, Ph.D, Professor
Mechanical Systems Lab
Department of Mechanical Engineering
University of Delaware, Newark DE 19716.
Email: agrawal@me.udel.edu

***Abstract*— Existing approaches for control of mobile robots using potential theory emphasize construction of local minimum free navigation functions in the configuration space. This is generally analytically complex and fails when nonholonomic constraints are introduced for a finite sized mobile robot. This paper approaches the issue by decoupling the problem into two parts: (1) Generating a non-analytical local minimum free navigation function based on the workspace obstacles. (2) Trapping the nonholonomic unicycle in a *local virtual* potential field and then moving this local field along the path generated in the first step. This results in the trapped robot following the generated path. The emphasis here is on following a geometric path. No explicit parameterization of this path to a time-trajectory is done. Convergence and stability issues due to the presence of nonholonomic constraints are addressed. Simulation and experimental results are provided.**

I. Introduction

The ubiquitous use of wheeled mobile robots (WMR's) has prompted their extensive study in the last two decades: see, for example, [24], [25], [11] and the references therein. In this paper, a simplified *dynamic* model of a unicycle is used. A smooth control law for its stabilization to a lower dimensional sub-manifold of the configuration space is derived. This result is later used to derive a path-following control law. A non-analytical local minimum free potential function (also called a navigation function) is used to create this path. The problem is formulated in such a way that it lends itself to a real-time solution and complex analytical expressions are avoided. This result is useful when a holonomic path along with the clearances to obstacles around it, are known and the robot is supposed to follow the path while using the clearance area to compensate for its nonholonomic equality constraints.

In this paper, it is assumed that robot's planar dimensions are about equal, i.e. elongated geometries are not considered. Inequality constraints, like steering angle limits are not considered. This implies that the unicycle's ability to rotate in place is assumed.

The organization of this paper is as follows: A brief review of the past work in the field of WMR's planning, control laws for stabilization, trajectory-tracking, path-following control, and potential theory, with an emphasis on their application to WMR's is presented in Sec. II. A methodology for representing the robot and the environment as bodies consisting of overlapping rings of virtual charge and a closed form computation of virtual forces and torque based on such a representation is presented in Sec. III. A computation of a feasible path in the form of a chain of rings of different sizes, is presented in Sec. III-A. The dynamic model of the unicycle is explained in Sec.IV. The behavior of a unicycle trapped in such a virtual static ring is analyzed in Sec. V. These results are then extended in Sec. VI to a virtual ring following the path found in Sec. III-A and having a unicycle trapped inside. Simulations and experimental results are also included. Finally, Sec. VII offers concluding remarks.

II. Literature Review

A. Planning and Control

The problem of open-loop planning of WMR's has been addressed, among others, in [12] using sinusoidal inputs and in [25] using a graph search in configuration space.

Brockett's theorem [1] states that systems like wheeled robots with non-integrable no-slip constraints cannot be stabilized to a point in the configuration space using a time-invariant C^1 feedback control law. However, such systems have been shown to be strongly accessible and small-time locally controllable at the origin of the state-space [6] using differential geometric approaches. The main control approaches for *stabilization* of nonholonomic WMR's could be categorized as:

1) *Time-varying smooth feedback control*: An extraneous time-varying component is introduced in the system to stabilize it using smooth feedback: Samson ([2]). This approach however results in slow convergence rate and oscillatory behavior which is not part of the original system. Recently, exponential stabilization was reported by Tian et al [5].
2) *Discontinuous feedback control*: This is by far the more popular approach. Bloch et al [6] use piecewise smooth analytical feedback and also showed that the system can always be stabilized to an $m-$dimensional manifold by smooth feedback where m is the number of nonholonomic constraints. Astolfi [8] obtained exponential stabilization by creating a discontinuity at the origin using a coordinate transform. A similar result was also obtained by de Wit et al [4].

Time-trajectory tracking was formulated using feedback linearization by [24] and using sliding mode control by [3]. Trajectory-tracking can usually be done as long as the robot keeps moving. The concept of time-parameterization (scaling) of a path for holonomic robots to meet the input constraints was introduced by Hollerbach [21]. It was extended to nonholonomic robots by [22] and was studied again in [23]. The path-following of a control point on the robot was addressed by [11]. *In this paper, the path-following control of a unicycle is addressed. This problem has been studied less extensively than trajectory-tracking*.

B. Potential Theory for WMR's

Potential theory, first introduced by Khatib [13], is attractive as it solves the planning and control problem simultaneously. Navigation functions were subsequently introduced ([16],[15],[17]) which did not have the problem of local minima. Most navigation functions are however analytically involved. Some numerical

navigation functions are discussed in [25]. Most of the current literature however focuses on holonomic robots. Potential theory applications for nonholonomic robots have been studied by Kyriakopoulos et al [20] where an obstacle free path was first found by classical methods and this path was time-parameterized. The resulting time-trajectory was then followed by a trajectory-tracking controller. In Tanner et al [19], a *kinematic* model of the unicycle is used and then a sliding-mode like controller is used to stabilize the system to the origin which is the global minimum of a potential function. This approach suffers from chattering and also cannot be readily generalized to a *dynamic* model. Recently, Tanner et al [7] have derived a strategy based on non-smooth Lyapunov functions and diffeomorphic transforms first introduced by [17]. Another approach [18] used in planning was to locally deform the holonomic paths by adding a cost which favors directions easier for the nonholonomic system.

III. Potentials Based on Rings

We consider a potential based on the inverse square law as it gives closed form analytic expressions for bodies composed of a union of overlapping rings. The word *charge* is loosely used to mean a virtual non-physical charge which gives rise to such a potential. For two Point *Charges* q_1, q_2, the potential energy is given by $V_p = \frac{q_1 q_2}{r^2}$, where r is the inter-charge distance.

Consider a point charge q and a uniformly charged ring of radius R with uniform charge density $\lambda = Q/(2\pi R)$. If q is at a distance d from the center of the ring, then one can use complex residue theorem to compute the potential energy V_d of the system.

$$V_d = \int_0^{2\pi} \frac{q\lambda R d\theta}{R^2 + d^2 - 2Rd\cos\theta} = \frac{qQ}{\mid R^2 - d^2 \mid} \tag{1}$$

This integral is singular when the point charge is on the ring ($d = R$).

Consider two uniformly charged rings with total charges Q_1, Q_2. The rings are of radii R_i and R_j, with their centers at distance c_{ij}. The potential energy of this system can be computed by integrating Eqn. 1 using the residue theorem:

$$V_{R_i R_j} = \int_0^{2\pi} \frac{2\pi\lambda_i\lambda_j R_i R_j d\theta}{\mid {R_i}^2 - {R_j}^2 - c_{ij}^2 + 2c_{ij}R_j\cos\theta \mid} \tag{2}$$
$$= \frac{Q_1 Q_2}{\sqrt{2\left({R_i}^4 + {R_j}^4 + c_{ij}^4\right) - \left({R_i}^2 + {R_j}^2 + c_{ij}^2\right)^2}}$$

where $\lambda_i \equiv Q_i/(2\pi R_i)$. This integral is singular for: $\mid R_i - R_j \mid \leq c_{ij} \leq R_i + R_j$. The singularity corresponds to the case when the rings are touching or intersecting each other. The result is clearly symmetric in R_i and R_j and is a property of the configuration.

Now we consider a *ring-world* where the robots and the environment are made up of overlapping rings. This representation can be found using a circle fitting algorithm (Algo. III.1). An example of a rigid 2D body composed of such rings is shown in Fig.1.

An advantage of this discretization is that the resolution (minimum ring size R_s) can be changed easily in the circle-fitting algorithm and no 'holes' are left. This algorithm is a simple variant of the bubble-expansion algorithm of [14].

The object's boundary is initially given by a set of points Γ that are closer together than the resolution (R_s) of the algorithm. The starting point ($\mathbf{r_s} = (x_s, y_s)$) is generally taken as a point within the body (generally the centroid). Each bubble-ring begets other children bubbles at its boundary which are as big as possible. The children are then put in a priority-queue which is prioritized by the clearance visible to that bubble. The notation $\mathcal{B}(\mathbf{r}, R, \mathcal{B}_p)$ denotes a bubble-ring of radius R with center at $\mathbf{r} = (x, y)$ and a parent bubble $\mathcal{B}_p$. R_s is the resolution or the radius of the smallest ring desired. The boundary Γ of the object is discretized to a set of points $\mathbf{q} \in \Gamma$.

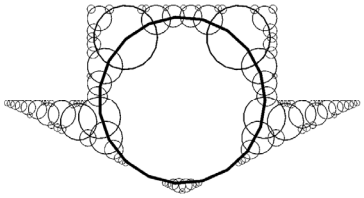

Fig. 1. A downward facing arrow composed of rings. This representation has been found using the circle-fitting algorithm Algo. III.1.

Algorithm III.1: FillRings($\Gamma, R_s, \mathbf{r_s}$)

Initialize priority queue Q, Initialize tree T
Compute $R_b = \overset{Min}{\mathbf{q}\in\Gamma} \|\mathbf{q} - \mathbf{r_s}\|$
$\mathcal{B} = (\mathbf{r_s}, R_b, NULL)$
Insert $\mathcal{B}$ in Q with priority R_b
while Q is not empty
do
- Pop Q into $\mathcal{B} = (\mathbf{r}, R, \mathcal{B}_p)$
- Insert $\mathcal{B}$ in T with parent $\mathcal{B}_p$
- Find n points $\mathbf{p_i}$ on the boundary of $\mathcal{B}$ by random/uniform sampling
- Delete $\mathbf{p_i} \subset \mathcal{B}_j \in (T \cup Q)$
- Compute $R_i = \overset{Min}{\mathbf{q}\in\Gamma} \|\mathbf{q} - \mathbf{p_i}\|$
- **if** $R_i > R_s$
  - **then** Insert $\mathcal{B}_i = (\mathbf{p_i}, R_i, \mathcal{B})$ in Q with priority R_i

return (T)

The rings concentrate at places where the geometry is complex. In this ring-world, which is reminiscent of the disk-world of [17], one composite-ring object affects other such objects. The potential-energy due to the interaction of rings within a single object is not important in this formulation because it does not affect the dynamics of inter-object interaction.

Let a composite object $\mathcal{O}_c$ be defined by the coordinates of a designated center (x_c, y_c) in a global referential and its orientation by the angle β_c of its *front* (axis $\mathbf{u}$) with respect to the global X axis. This is illustrated in Fig. 2. To further define the shape of the object $\mathcal{O}_c$, the parameters $(r_i, \theta_i, R_i)_C$ for each of its constituent rings ($i = 1 \cdots n$) are given. (r_i, θ_i) are the polar coordinates of the center of the ith ring in object C-fixed coordinates, and R_i is the radius of the ring.

To find the virtual forces acting on the composite-object ($\mathcal{O}_c$) the gradients of the total potential energy of the system V_Σ with respect to the d.o.f's of the object i, namely, $\frac{\partial V_\Sigma}{\partial x_c}$, $\frac{\partial V_\Sigma}{\partial y_c}$, $\frac{\partial V_\Sigma}{\partial \beta_c}$ need to be computed. This can be done as follows:
Let V_{Σ_c} denote the part of V_Σ to which $\mathcal{O}_c$ contributes. Then $\frac{\partial V_\Sigma}{\partial x_c} = \frac{\partial V_{\Sigma_c}}{\partial x_c}$ etc. hold.

Let (x_o, y_o, R_o) denote a ring $\notin \mathcal{O}_c$, with its center at (x_o, y_o) in global coordinates and with radius R_o. Let c_{io} be the distance between the center of ring $i \in \mathcal{O}_c$ and (x_o, y_o). The force/torque on $\mathcal{O}_c$ due to the external objects can be computed by the following algorithm (see Fig. 2):

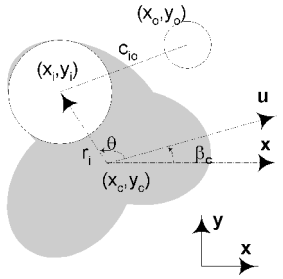

Fig. 2. The coordinate system of object C ($\mathcal{O}_c$), with an external ring shown.

Algorithm III.2: FORCESON($\mathcal{O}_c$)

$V \equiv V_{\Sigma_c} \leftarrow 0$,
$\frac{\partial V}{\partial x_c} \leftarrow 0$, $\frac{\partial V}{\partial y_c} \leftarrow 0$, $\frac{\partial V}{\partial \beta_c} \leftarrow 0$
for each $(x_o, y_o, R_o) \notin \mathcal{O}_c$
do { **for each** $(r_i, \theta_i, R_i)_C \in \mathcal{O}_c$
do { **comment:** Using Eq.(2) for $V_{R_i R_o}$
$V \leftarrow V + V_{R_i R_o}$,
$\frac{\partial V}{\partial \beta_c} \leftarrow \frac{\partial V}{\partial \beta_c} + \frac{\partial V_{R_i R_o}}{\partial c_{io}} \frac{\partial c_{io}}{\partial \beta_c}$
$\frac{\partial V}{\partial x_c} \leftarrow \frac{\partial V}{\partial x_c} + \frac{\partial V_{R_i R_o}}{\partial c_{io}} \frac{\partial c_{io}}{\partial x_c}$
$\frac{\partial V}{\partial y_c} \leftarrow \frac{\partial V}{\partial y_c} + \frac{\partial V_{R_i R_o}}{\partial c_{io}} \frac{\partial c_{io}}{\partial y_c}$

where the following definitions are used:

$$x_i = x_c + r_i \cos(\beta_c + \theta_i), \quad y_i = y_c + r_i \sin(\beta_c + \theta_i),$$
$$\frac{\partial V}{\partial c_{io}} = \frac{2 Q_i Q_o c_{io} (R_i^2 + R_o^2 - c_{io}^2)}{\Delta^{3/2}},$$
$$c_{io} = \sqrt{(x_i - x_o)^2 + (y_i - y_o)^2},$$
$$\Delta \equiv 2\left({R_i}^4 + {R_o}^4 + c_{io}^4\right) - \left({R_i}^2 + {R_o}^2 + c_{io}^2\right)^2,$$
$$\frac{\partial c_{io}}{\partial x_c} = \frac{x_i - x_o}{c_{io}} = a_x, \quad \frac{\partial c_{io}}{\partial y_c} = \frac{y_i - y_o}{c_{io}} = a_y, \tag{3}$$
$$\frac{\partial c_{io}}{\partial \beta_c} = -r_i \sin(\beta_c + \theta_i) a_x + r_i \cos(\beta_c + \theta_i) a_y. \tag{4}$$

Finally, one gets:

$$F_x = -\frac{\partial V_{\Sigma_c}}{\partial x_c}, \; F_y = -\frac{\partial V_{\Sigma_c}}{\partial y_c}, \; \tau_\beta = -\frac{\partial V_{\Sigma_c}}{\partial \beta_c} \tag{5}$$

which are the virtual force and torque acting at any instant on the composite body $\mathcal{O}_c$. Far away objects can either be ignored or only the biggest rings in them need to be considered. Due to closed form expressions these computations can be done in real-time. Finally, a virtual potential terrain can be setup to achieve a desired behavior from the system.

A. Searching Available Space

Given a robot's start and a goal position in a ring-world environment with ring-obstacles, we are interested in a method, which would find a feasible path in workspace while also characterizing the surrounding clearance at each point. The classical grid based methods are inefficient for this. Here a 2D adaptation of the 'bubble' expansion algorithm given in Brock et al [14] is used.

The basic algorithm is the same as Algo. III.1. The bubbles start expanding from the goal point (root of the search-tree) and the expansion continues till a bubble is found containing the goal point. The only difference from Algo. III.1 is that the priority queue is prioritized by the distance of a bubble from the start point. This means that the bubble closest to the start point is allowed to be expanded first. After the algorithm terminates, the branch of the tree containing a leaf node with the start point, is a feasible path. If each node in this branch is given a 'potential' equal to its depth in the tree, it defines a local minimum free navigation function from the start to the goal point [14].

A sample run is given in Fig.3. The minimum 'bubble' size should be greater than the actual robot radial size. This planning algorithm can be repeatedly run in a dynamic environment. The centers of the resulting 'bubbles' are joined by a smooth interpolating curve, which gives us the path to be tracked. This would be made use of in the path-following control discussed in Sec.VI.

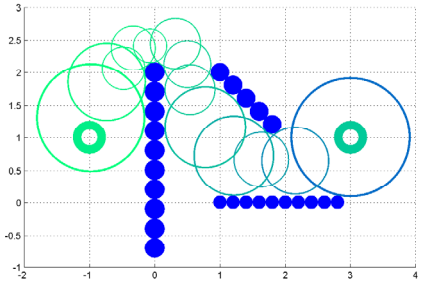

Fig. 3. A 'bubble' path: filled circles are obstacles, doughnuts are the start and the goal positions. The remaining rings are the bubbles found by the algorithm where the size of the ring represents the radial clearance.

IV. UNICYCLE DYNAMIC MODEL

The dynamic model for the unicycle used is a simplified version of the model presented in [11]. It has been assumed that the inertial quantities for the two wheels are negligible compared to those of the robot platform. Let $\mathbf{q} = [x_c, y_c, \phi]^T$ be the configuration variables, where x_c, y_c are the coordinates of the center of mass of the robot in a global referential and ϕ denotes its orientation (see Fig. 4). The inputs to the system are the motor torques on the two wheels. The nonholonomic no slip constraint can be given by:

$$A(\mathbf{q})\dot{q} = 0, \; A(\mathbf{q}) = [\sin(\phi), -\cos(\phi), 0]. \tag{6}$$

The null-space of $A(\mathbf{q})$ is:

$$S(\mathbf{q}) = \begin{pmatrix} \cos(\phi) & 0 \\ \sin(\phi) & 0 \\ 0 & 1 \end{pmatrix}. \tag{7}$$

Let the heading velocity of the robot be v and the turning velocity be $\dot{\phi}$ The system dynamic equations can be written as:

$$\nu = \begin{pmatrix} v \\ \dot{\phi} \end{pmatrix}, \mathbf{x} = \begin{pmatrix} \mathbf{q} \\ \nu \end{pmatrix}, \; \dot{\mathbf{q}} = S(\mathbf{q})\nu \tag{8}$$

$$\dot{\mathbf{x}} = \begin{pmatrix} S\nu \\ \mathbf{f} \end{pmatrix} + \begin{pmatrix} \mathbf{0} \\ (S^T M S)^{-1} S^T E \end{pmatrix} \tau, \tag{9}$$

$$M = \begin{pmatrix} m & 0 & 0 \\ 0 & m & 0 \\ 0 & 0 & I \end{pmatrix}, \tau = \begin{pmatrix} \tau_r \\ \tau_l \end{pmatrix}, \tag{10}$$

$$E = \begin{pmatrix} \cos(\phi)/r & \cos(\phi)/r \\ \sin(\phi)/r & \sin(\phi)/r \\ R/r & -R/r \end{pmatrix},$$
$$\mathbf{f} = -(S^T M S)^{-1}(S^T M \dot{S})\nu. \tag{11}$$

where m is the mass and I is the moment of inertia of the platform. τ_r is the motor torque on the right wheel and τ_l, that on the left.

$2R$ is the distance between the wheels and r is the radius of each wheel. In our case, simple calculations show that $\mathbf{f} = 0$.

According to the third condition given in Brockett's theorem in [1], the mapping

$$(\mathbf{q}, \tau) \rightarrow (S\nu, (S^T M S)^{-1} S^T E \tau) \tag{12}$$

should contain a neighborhood of $\mathbf{0}$. This is not satisfied at points such as: $(\dot{q}_d, (S^T M S)^{-1} S^T E \tau)$ where $A(\mathbf{q})\dot{q}_d \neq 0$ are not present in the range of the mapping. This system therefore is *not* asymptotically stabilizable to a point. It is however stabilizable to a 1 dimensional manifold $N_e = \{(\mathbf{q}, \dot{\mathbf{q}}) | \dot{\mathbf{q}} = 0, \mathbf{s}_{2\times 1}(\mathbf{q}) = 0\}$ [6].

V. Stabilization Using an External Static Virtual Ring

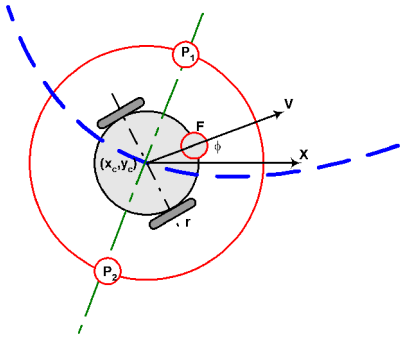

Fig. 4. A unicycle inside a virtual ring

Let the robot be trapped in a static virtual ring of an arbitrary charge distribution (see Fig. 4). Let us consider the robot itself to be a charged ring with a certain charge density along its periphery. The charge distribution between the robot and the outer ring gives rise to a potential energy of the system denoted by $U_\Sigma(\mathbf{q})$. Since the outer ring is at rest, we set its configuration variables $\mathbf{q_o} = 0$.

We would like to investigate smooth control laws based on charge-interactions and the equilibrium configuration manifolds of the robot inside the outer ring. The initial configuration of the robot is completely inside the outer ring and it has arbitrary heading and turning speeds. This initial state is given by $\mathbf{x_0}$. We then consider a candidate Lyapunov function:

$$V(\mathbf{x}) = U_\Sigma(\mathbf{q}) + (1/2)\nu^T (S^T M S)\nu \tag{13}$$

$S^T M S$ is positive definite and in our case it is diag(m, I).

$$\dot{V} = \frac{\partial U_\Sigma}{\partial \mathbf{q}}^T S\nu + \nu^T (S^T E \tau). \tag{14}$$

The control law is chosen as:

$$S^T E \tau = -S^T \frac{\partial U_\Sigma}{\partial \mathbf{q}} - K\nu, \tag{15}$$

$$\dot{V}(\mathbf{q}, \nu) = -\nu^T K \nu \leq 0. \tag{16}$$

In the present case $S^T E$ is a full rank square matrix and we can always find τ This shows that $V(\mathbf{x})$ is a non-increasing function and the robot stays within the closed set $S = \{\mathbf{x} | V(\mathbf{x}) <= V(\mathbf{x}_0)\}$. If the robot periphery were to intersect the outer ring, V would become unbounded and therefore it would mean that the robot state has gone out of set S. This shows that the robot is trapped in the ring and would come to rest within the ring.

To find the equilibrium states, one uses LaSalle Invariant Set Theorem [10]. The Invariant set corresponds to:

$$\nu = 0, \quad S^T \frac{\partial U_\Sigma}{\partial \mathbf{q}} = 0 \tag{17}$$

Eqn.(17) gives two conditions and therefore the system pose $\mathbf{q}$ can be stabilized to a 1 dimensional manifold. These conditions are:

$$\frac{\partial U_\Sigma}{\partial \phi} = 0, \quad \frac{\partial U_\Sigma}{\partial x}\cos(\phi) + \frac{\partial U_\Sigma}{\partial y}\sin(\phi) = 0 \tag{18}$$

This means that at equilibrium, the net torque should be zero and the net force should be parallel to the wheels' axis. Such a manifold is shown for some charge distributions of the inner and outer ring in Fig. 5. These also happen to be the chattering surfaces in the discontinuous control law based on a kinematic model in [19].

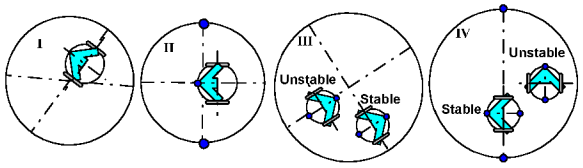

Fig. 5. Four different charge distributions and their equilibrium states

In the equilibrium states illustrated in Fig. 5, the peripheral charge along the ring is taken to be much smaller than the point-charges denoted as filled circles. For most cases, an equilibrium in one orientation also implies an equilibrium in an orientation with the front and the back of the robot reversed. The equilibrium configurations can be found by evaluating Eq. 18 using Algo. III.2. In most cases analytical solution is difficult and a numerical search is employed. In most of the arguments presented, an exact solution is not required and visualization of forces and torques can be used as an aid.

In part I of Fig. 5, both the robot and the outer ring have only uniform charge density along the perimeter. In this case no torque acts on the robot and it settles down in a configuration where the wheels' axis is parallel to a diameter of the outer ring. In this case the net force pushing the robot to the center of the external ring is parallel to the wheels' axis.

In part II of Fig. 5, apart from the uniform charge density, the robot has a point charge at its front. The external ring also has two point charges along a diameter. Note that there is no *stable* equilibrium such that the wheels' axis are perpendicular to the external ring's diameter containing the point-charges. This fact is made use of in Sec. VI

In part III of Fig. 5, apart from the uniform charge density, the robot has two point charge at its front and back. Now a torque acts on it and it is zero only when either the front is aligned along a diameter or is perpendicular to one, consequently these are the equilibrium positions. However the position where the point charges are along the diameter have been analytically found to be unstable.

In part IV of Fig. 5, both the robot and the outer ring have two additional point charges each along a diameter. The torque is now zero only along the diameter of the outer ring containing its point charges (the y-axis), and along an orthogonal diameter (x-axis). Along the x-axis $\phi = \pi/2$ is an (unstable) equilibrium, whereas

along the y-axis, $\phi = 0$ is a (stable) equilibrium. This has been determined using a numerical search in the configuration space for the solution of Eqs.(18).

In all the above cases, the origin is the global minimum but due to the nonholonomic constraint, the robot could get stuck in the above mentioned manifolds and they can be escaped only by a discontinuous feedback law.

VI. Path-following using an Exterior Moving Ring

We use the fact that part IV of Fig.5 always provides the right values of alignment and of at least one other coordinate ($\phi = 0, x = 0$). This is utilized in deriving a control law for following a path whose equation is given in a parametric form with the parameter p. This path is obtained by the method in Sec.III-A and could be periodically refreshed. The size of the outer virtual ring is determined by the diameter of the clearance 'bubble'. The path is divided into segments where the 'bubble' size remains about the same and the outer virtual ring size is chosen as that of the smallest 'bubble' in that segment. In the following we consider one such segment.

The outer virtual ring moves along the path towards the goal ($p = 0$) and while dragging the robot along. The robot applies a drag force on the outer ring as it moves. We now need to show that the outer ring in fact reaches the destination. *The two point charges of the outer ring always stay normal to the path being traversed.* Let the pose variable (x_c, y_c, ϕ) of the outer ring be denoted by $\mathbf{q_o}$ and that of the robot by $\mathbf{q}$. The control input variable for the outer-ring is the force f_t tangent to the path which drags it towards the goal. The following simple dynamic equation is used for the virtual ring.

$$\mathbf{q_o} = [x(p), y(p), \tan^{-1}(y'(p)/x'(p))], \ \ddot{p} = f_t. \tag{19}$$

The following Lyapunov function is used:

$$V(\mathbf{x}, \mathbf{x_o}) = U_\Sigma(\mathbf{q}, \mathbf{q_o}) + \frac{1}{2}\nu^T(S^T M S)\nu + \frac{1}{2}K_p p^2 + \frac{1}{2}\dot{p}^2 \tag{20}$$

$$\dot{V} = \frac{\partial U_\Sigma}{\partial \mathbf{q}}^T S\nu + \frac{\partial U_\Sigma}{\partial \mathbf{q_o}}^T \frac{d\mathbf{q_o}}{dp}\dot{p} + \nu^T S^T E\tau + K_p p\dot{p} + \dot{p}f_t \tag{21}$$

The control law chosen is:

$$S^T E\tau = -S^T \frac{\partial U_\Sigma}{\partial \mathbf{q}} - K_s\nu,$$

$$f_t = -\frac{\partial U_\Sigma}{\partial \mathbf{q_o}}^T \frac{d\mathbf{q_o}}{dp} - K_p p - K_v\dot{p}. \tag{22}$$

$$\dot{V} = -\nu^T K_s \nu - K_v \dot{p}^2 \leq 0 \tag{23}$$

Applying LaSalle's Invariant Set Theorem again for this system, one gets at equilibrium:

$$\nu = 0, \ \ S^T \frac{\partial U_\Sigma}{\partial \mathbf{q}} = 0 \tag{24}$$

$$\dot{p} = 0, \ \ \frac{\partial U_\Sigma}{\partial \mathbf{q_o}}^T \frac{d\mathbf{q_o}}{dp} = -K_p p \tag{25}$$

Note that the control law derived is independent of the inertial parameters of the robot and therefore no explicit parameter adaptation needs to be added as in [9]. Eq.(24) is similar to the one in Sec.V. Eq.(25) states that the attraction of the outer ring towards $p = 0$ should be the same as the drag caused by the robot trapped within at equilibrium. The value of K_p is critical. It should be high enough to get the system started. As K_p increases, the accuracy of the path-tracking decreases and the total time to traverse the path also decreases. This is illustrated in Fig. 6 and Fig. 7. Since the two point charges of the outer ring always stay normal to the path being traversed, the robot cannot come to an equilibrium such that its wheels axis is parallel to the path and thus the trapped robot will not block the outer virtual ring. Its static equilibrium is always such that it is oriented along the path. The system can thus not get trapped midway and the outer-ring does reach the point $p = 0$. For the last segment of the path, the virtual outer ring's size should be close to that of the robot to ensure a convergence near the desired goal configuration.

A simulation result is shown in Fig. 6. The path to be followed is parameterized as: $x = s, y = \sin(2\pi s/s_f)$. It is interesting to see that during sharp turns, the outer ring's speed automatically decreases until the robot aligns itself along the new traveling direction. If the robot motor torques saturate, the outer ring has to again decrease its speed due to the increased drag caused by the robot. On straight stretches, the speed picks up.

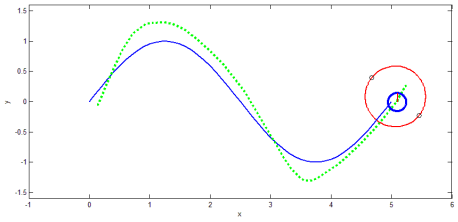

Fig. 6. Path-following control simulation on a path-segment having a constant outer virtual ring size. The charge-configuration was as shown in Fig. 4. The robot's periphery is a charged ring with a point charge at its front. The dotted line shows the actual path of the robot's center, whereas the solid line shows the reference sinusoidal path. $K_p = 5$, Path-traversal time= 5 sec.

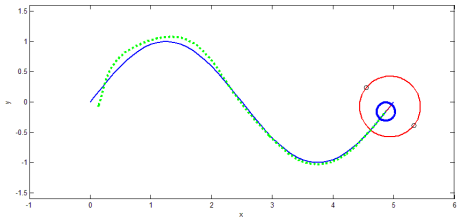

Fig. 7. This figure shows that the path-tracking can be significantly improved by lowering K_p. $K_p = 0.5$, Path-traversal time= 25 sec. Compare with Fig. 6.

A. Experiment

For the experiment an IRobot's Magellan Pro unicycle was employed. Since the control programmatic interface only allows set points for the heading speed v and turning speed $\dot{\phi}$ to be specified at each sampling interval, a variant of the above strategy was used. The robot odometry was sampled for the robot's configuration at each instant. The dynamic equations of the outer virtual ring and the robot as given previously were integrated for one sampling period by using the motor torques as computed by the Eq.23 and the current system state. The result of integration gives the new $v, \omega = \dot{\phi}$ which are given as the new set-points. The experimental setup is shown in Fig. 8.

The experimental data is plotted in Fig. 9. The results show that the path was followed within the spatial freedom allowed. The robot is not exactly tangential to the desired path at each point. This offset is due to the fact that the charge configuration IV of

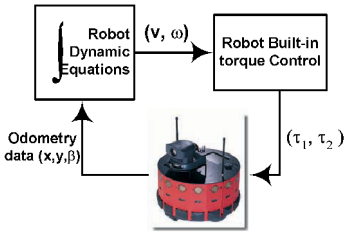

Fig. 8. The experimental setup

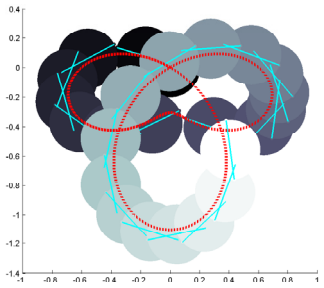

Fig. 9. The experimental plot. The area swept by the robot is denoted by colored disks whose color gradient denotes the time progression. The orientation is denoted by a diameter of the circle. The reference path is denoted by the dotted red line. The virtual external ring was twice the size of the robot and charge configuration IV of Fig. 5 was used.

Fig. 5 was used. The equilibrium manifold of this configuration is such that the robot is oriented perpendicular to the diameter containing the two point charges on the external ring.

VII. Conclusions

A novel practical method of path-following control of a circular unicycle is introduced. The representation of the environment as well as computation of feasible paths is done using rings in $2-D$. The technique involves surrounding the robot with a local virtual potential field with known minima and computing the robot inputs based on it. Only continuous control is considered and the robot is controlled to follow an obstacle-free geometric path found in a prior step. No explicit time parameterization of the path (trajectory generation) is required and the speed of path traversal can be controlled by tuning some control parameters. This technique is useful because due to the presence of nonholonomic constraints a feasible time-trajectory is difficult to find.

Further work needs to be done for arbitrary shaped nonholonomic robots having inequality constraints on inputs. An extension of this approach to multiple-robot groups is being explored.

VIII. Acknowledgments

The authors appreciate financial supports of NSF Award No. IIS-0117733, NIST MEL Award No. 60NANB-2D0137, PTI/NIST Award No. AGR20020506, NSF UAV Award and NIST Award No. SB 1341-03-W-0338.

References

[1] Brockett, R.W. “Asymptotic Stability and Feedback Stabilization”, *Differential Geometry Control Theory*, Edited by Brockett, R.W. et al, Progress in Mathematics, Vol. 27, Birkhäuser, 1983.

[2] Samson, C. “Time-varying Feedback Stabilization of Car-like Wheeled Mobile Robots”, *Int. Journal of Robotics Research*, Vol. 12, No.1, Feb. 1993.

[3] Yang J-M., and Kim J-H. “Sliding Mode Control for Trajectory Tracking of Nonholonomic Wheeled Mobile Robots”, *IEEE Trans. Robotics and Automation*, Vol. 15, No.3, June 1999.

[4] de Wit, C. C., and Sordalen, O.J. “Exponential stabilization of mobile robots with nonholonomic constraints.”, *IEEE Trans. on automatic control*, Vol. 37, No. 11, Nov. 1992.

[5] Tian, Y-P., and Li, S. “Exponential stabilization of nonholonomic dynamic systems by smooth time varying control”, *Automatica*, Vol. 38, 2002.

[6] Bloch, A.M., Reyhanoglu, M. and McClamroch, N.H. “Control and Stabilization of Nonholonomic Dynamic Systems”, *IEEE Transactions on Automatic Control*, Vol. 37, No. 11, Nov. 1992.

[7] Tanner, H.G., Loizou, S.G., and Kyriakopoulos, K.J. “Nonholonomic Navigation and Control of cooperating mobile manipulators”, *IEEE Trans. on Robotics and Automation*, Vol. 19, No. 1, 2003.

[8] Astolfi, A. “Asymptotic Stabilization of Nonholonomic Systems with Discontinuous Control”, *Ph.D Dissertation, Swiss Federal Institute of Tech., Zurich*, 1996.

[9] Aguiar, A. P., Atassi, A. N., and Pascoal, A. M. “Regulation of a Nonholonomic Dynamic Wheeled Mobile Robot with Parametric Modeling Uncertainty using Lyapunov Functions”, *IEEE Conf. on Decision and Control, Sydney*, 2000.

[10] Slotine, J-J., and Li, W. “Applied nonlinear control”, *Prentice Hall*, 1991.

[11] Sarkar, N., Yun, X., and Kumar V. “Control of Mechanical Systems with Rolling Constraints: Application to dynamic control of mobile robots”, *Int. Journal of Robotics Research*, Vol. 13, No. 1, Feb. 1994.

[12] Murray R. M., and Sastry, S.S. “Nonholonomic Motion Planning: Steering Using Sinusoids”, *IEEE Trans. on Automatic Control*, 38(5):700–716, May 1993.

[13] Khatib, O. “Real-Time Obstacle Avoidance for Manipulators ”, *The International Journal of Robotics Research*, Vol. 5, No. 1, 1986.

[14] Brock, O. , and Kavraki, L.E. “Decomposition-based motion planning: A framework for real-time motion planning in high-dimensional configuration spaces”, *IEEE ICRA*,v 2, 2001, p 1469-1474.

[15] Kim, Jin-Oh, and Khosla, P. K. “Real-Time Obstacle Avoidance Using Harmonic Potential Functions”, *IEEE Tr. on Robotics and Automation*, June 1992.

[16] Akishita, S., Kawamura, S., Hayashi,. “Laplace potential for moving obstacle avoidance and approach of a mobile robot.”, *Japan-USA Symposium on flexible automation, A Pacific rim conference.*, 1990.

[17] Rimon, E., and Koditschek, D.E. “Exact Robot Navigation using Artificial Potential Fields”, *IEEE Trans. Robotics and Automation*, Vol. 8, No. 5, Oct. 1992.

[18] Sekhavat, S., and Chyba, M. “Nonholonomic deformation of a potential field for motion planning”, *Proc. of 1999 IEEE ICRA*, 1999.

[19] Tanner, H.G., and Kyriakopoulos, K.J. “Nonholonomic Motion planning for mobile manipulators”, *Proc. 2000 IEEE ICRA*, April 2000.

[20] Kyriakopoulos, K.J., Kakambouras, P., and Krikelis, N.J. “Potential Fields for Nonholonomic Vehicles”, *IEEE Int. Symp. on Intelligent Control*, Monterey, CA, 1995.

[21] Hollerbach, J. M. “Dynamic Scaling of Manipulator Trajectories”, *Journal of Dynamic Systems, Measurement and Control*, Vol. 106, 1984.

[22] Graettinger, T.J., Krogh, B.H. “Evaluation and Time-scaling of trajectories for wheeled mobile robots.”, *Transactions of the ASME*, Vol. 111, June 1989.

[23] Antonelli, G., Chiaverini, S., and Fusco, G. “Real-Time Path Tracking for unicycle-like mobile robots under velocity and acceleration constraints.”, *American Control Conference*, Arlington, VA, 2001.

[24] d’Andrea-Novel, B., Campion, G., and Bastin, G. “Control of Nonholonomic Wheeled Mobile Robots by State Feedback Linearization”, *The Int. Journal of Robotics Research*, Vol. 14, No. 6, Dec. 1995.

[25] Latombe J.-C. “Robot Motion Planning.”, *Kluwer Academic Publishers*, 1991.